Published by :
http://www.ijert.org

International Journal of Engineering Research & Technology (IJERT)
ISSN: 2278-0181
Vol. 6 Issue 07, July - 2017

Design and Analysis of an Amphibian Inspection Robot

Pasala Venkata Satish
Mechanical Engineering
Pydah Kaushik College of engineering & technology,
Vishakhapatnam, India.

***Abstract*— Accidents due to pipe leakage become extremely noticeable now-a-days. It is due to the very large and long pipe lines with different geometry makes hard to examine, hence this complex task can be easily done by In-pipe robots. But the robots need absolutely perfect kinematics to navigate. Hence this new mechanism and design allows the robot to travel in reduced branch pipes and branch pipes with zero-radius of curvature, which are common in real life and they pose a challenge to the previously developed in-pipe robots.**

This paper deals with a design and motion planning of an In-pipe robot. The robots which are currently on move don't possess ability to travel in pipe while medium is on stream, thus this robot is planned with a specific end goal to conquer this issue. This is an amphibious robot hence it can travel in both liquid and gaseous environment.

Keywords*— *Inspection Robot, Kinematics, Optimal Design, Pipeline Robot, Reconfigurable Robot, Motor Drives, Aurdino, Amphibian Robot.

I. INTRODUCTION

Pipelines are the medium through which large amount of fluids and gases are transferred from one place to other places every-day. Repairing those pipes has always a problematic due to geometrical and geographical difficulties. In-pipe robo inspection and repairing is a perfect solution for resolving this type of issues. In-pipe robots are classified in several ways. They are categorized as wheel track inch worm walking and pig depending on their kinematic mechanisms.

Using caterpillar wheel mechanism the robot can overcome the problem of kinematic restrictions which are occurred due to the complexity of the pipe geometries. Other robots like Flat robot [1] and snake robots [2] uses lot of servos and makes noises. The stability of these robots are quite less which makes them very less preferable, hence in this robot additional actuators like springs are used to stabilize the robots. This robot contains six motors and three of them are used to create forward motion of the robot and the other remaining motors are used to steer the robot.

The robot base wheels axis is not constant they can change its axis of orientation according to the pipe geometry and environment. This can be done with a special mechanism which is later explained in this paper in design section. This unique mechanism allows robot to navigate even in the most complex geometric environment of pipeline.

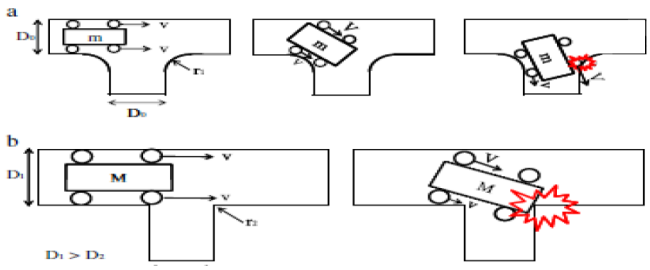

Fig 1.1: General design Problem encountered by a conventional in-pipe robot

A versatile in-pipe robot adjust to a channel's inward surface with springs just, no extra actuators are utilized. In-pipe robots that adjust to tunnels effectively, in any case, can travel more successfully than the robots with uninvolved adjustment in light of the fact that the typical power between the robot and the channel is controlled with extra actuators. A considerable lot of the created in-pipe robots can cross straightforward channel arrangements, for example, straight pipes or pipes with no variety in distance across. Albeit, a few robots can go through fanned and elbow channels, going in spread tunnels is still viewed as a test in the field of In-pipe apply autonomy. Indeed, even these robots that are intended to go through branched pipes.

Branches with zero span of arch Moreover, these robots require troublesome and confused velocity or control procedures to navigate these sorts of channels. Differential wheel drive sort robots are thought to be the best at going through branches. In any case, the accompanying issues can happen when these sorts of robots assess branch tunnels with the two previously stated conditions. The robot can get stuck in a zero-span of curvature and flow branch because of an absence of space for turning in the direst outcome imaginable the robot can collide with the edge of the branch, which may harm the robot.

The issues specified above may be exacerbated in a lessened branch tunnel. In-pipe robots intended for bigger channels are normally bigger and in this way heavier. Since differential wheel drive sort robots encounter some effect amid turning in a branch, an expansion in weight can generously decrease the robot's perseverance. Present another configuration for an essentially organized In-pipe robot with straightforward yet successful movement methodologies for going through reduced branch pipes and branches with zero range of curvature and flow and additionally vertical and elbow channels. This recently built up robot's movement through branches is not connected with accidents; in this way, this robot can go through bigger channels Conducted recreation studies to

International Journal of Engineering Research & Technology (IJERT)
ISSN: 2278-0181
Vol. 6 Issue 07, July - 2017

foresee the robot's capacities and to fabricate a model additionally directed trials with different tunnel setups to describe a model of our proposed In-pipe robot.

II. DESIGN AND ANALYSIS

A. Design of robot central body.

The robot which is designed in this paper is an amphibious robot i.e. it have capability to adapt design according to the environment in the pipes. For example, if the pipeline carries crude oil the robot arms are replaced with self-balanced propeller, the central body of the robot remains same for both. The focal body is intended to manage all hassles and it is planned efficiently to get by in both liquid and gasses environment. Accordingly with the assistance of the propellers it can explore in the fluid environment. Thus with the help of the propellers it can navigate in the liquid environment.

Balance and friction of the robot varies with vary in the medium of the pipeline, hence an amphibious robot is best preferred for in-pipe inspection. Its design allows to blend in with surrounding environment. With simple assembly steps and dissembling steps anyone can operate it with-out a special skills. This robot central body have 3 slot inputs at left side, right side and on top side which are shown in the figures from 2.1.1 to figure 2.1.3. In this slots the robot arms are fitted and screwed and in mode 2 same slots are fitted with propellers instead of arms. Hence with this design a single robot can handle dual environment without any help of other robots [2]. This key feature proves its versatility and other advantages.

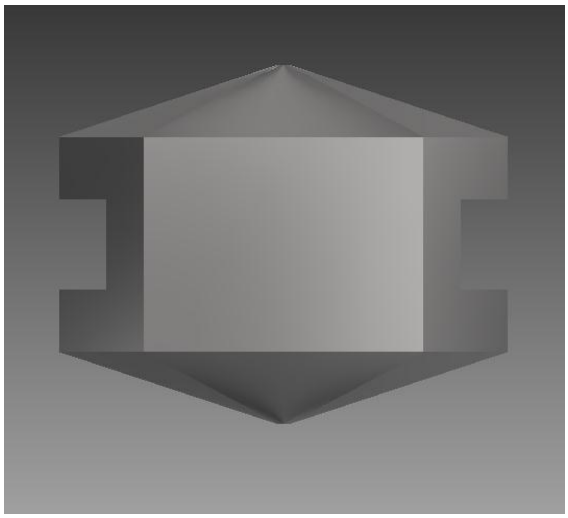

Fig 2.1.1: Bottom view of robot central body.

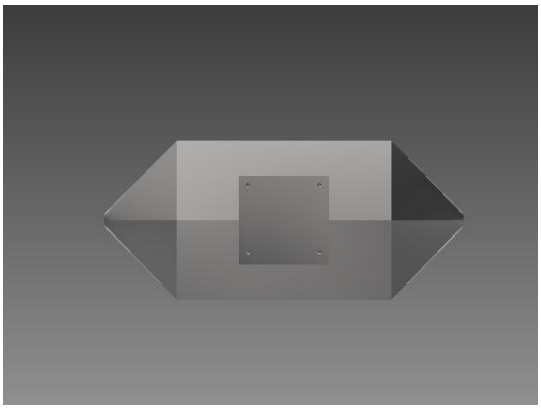

Fig 2.1.2: Right side view of robot central body.

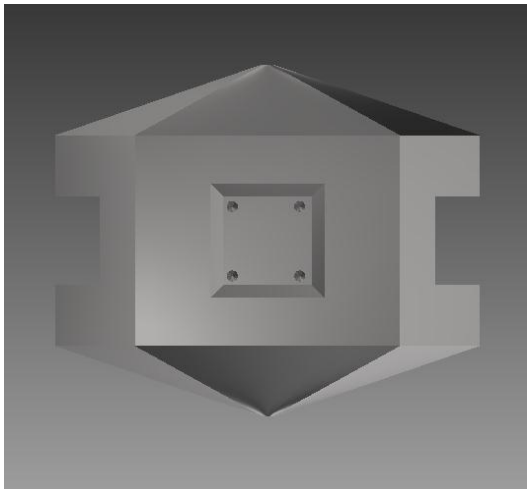

Fig 2.1.3: top view of robot central body

These are main views of robot central body. Further design details are show in the other section of the paper.

B. Design of other essential components.

1) Robot arm

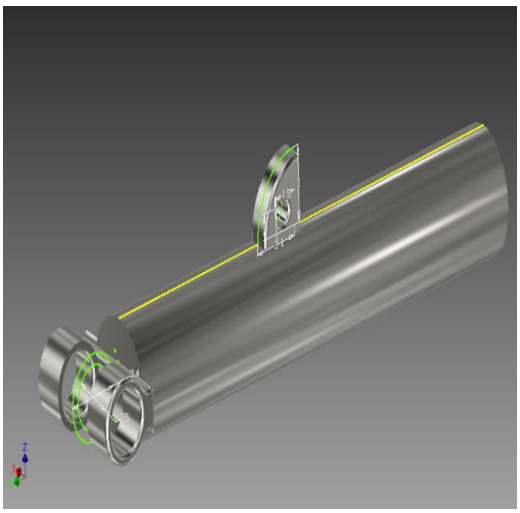

Fig: 2.2.1 Robot arm

This mechanism contains three limbs, which supports the robot. These three arms connected to the main body with the help of the semi-permanent base plates, these can removed or attached by simple screws. The design is shown in figure 2.2.1. These robot arms are well tested and analyzed in order to sustain the working pressure of the stream. The stress analysis results are positive. It can sustain at the working pressure and those simulation is shown in figure 2.2.2. The maximum stress concentration of 45 Mpa of pressure is observed at the junction of the arm and collar. When a maximum pressure of 500 newton's applied the deformation is very low i.e. less than 2 mm. this deformation cannot pose trouble to robot, hence this arm can be preferred for the robot

International Journal of Engineering Research & Technology (IJERT)
ISSN: 2278-0181
Vol. 6 Issue 07, July - 2017

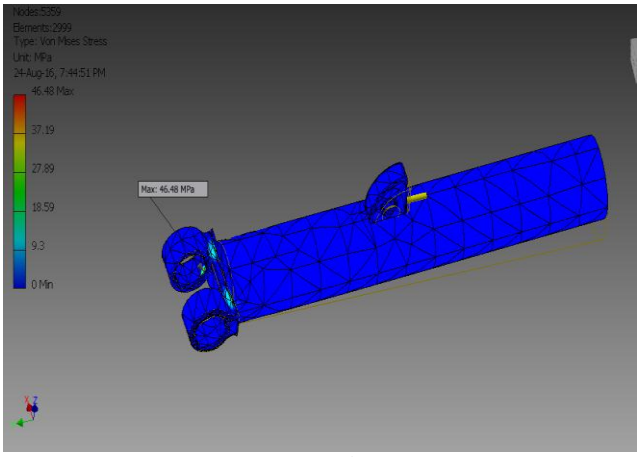

Fig: 2.2.2: Stress analysis of robot arm.

The extended part from the cylinder surface is used to connect the suspension and arm with Clevis pin. The whole stress will be concentrated at that area, hence in order to decrease stress concentration contact area is increased.

2) Suspension of robot arm for adittional actuation.

Fjg: 2.2.3 Suspension for robo arm.

The suspension system is used to maintain necessary traction force. Thus it helps to stabilize the robot motion in pipeline. Otherwise robot losses its grip in pipe line due to stream.

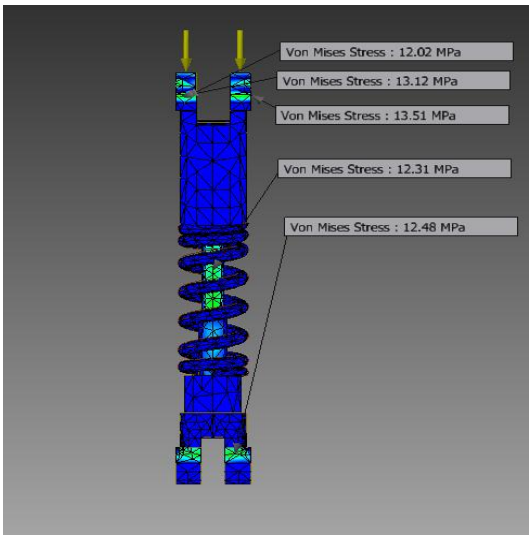

Fig: 2.2.4: Stress analysis of robot arm's suspension.

The stress analysis results are positive. It can sustain at the working pressure. The maximum stress concentration of 13 Mpa of pressure is observed at the junction of the arm and collar. When a maximum pressure of 500 newton's applied the deformation is very low i.e. less than 1 mm. this deformation cannot pose trouble to robot. The design and stress analysis simulation of suspension are shown in figure 2.2.3 and 2.2.4.

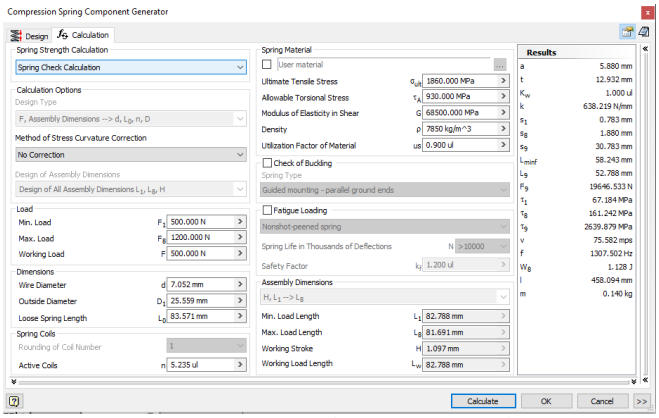

Fig: 2.2.5: calculation of robo arm's suspension

3) Caterpiller wheel base

This robot have to go through numerous elbows or T-junctions utilizing the Caterpillar wheels. A normal wheel system can't work appropriately in the pipeline with a little range of arch in light of the fact that, occasionally, the wheels lose contact with the surface. All Caterpillar wheels keep up contact with the surface of the pipeline. The robot works steadily as each Caterpillar works autonomously.

International Journal of Engineering Research & Technology (IJERT)
ISSN: 2278-0181
Vol. 6 Issue 07, July - 2017

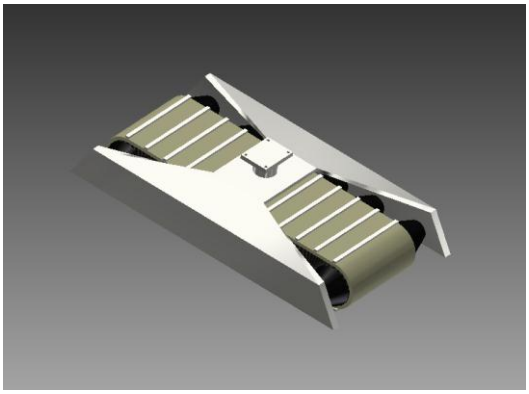

Fig 2.2.6: Caterpillar wheel base

And they are capable of withstanding uneven surface inside the pipeline. The best quality of Caterpillar wheels is that they maintain substantial contact zone for movements over unpredictable surfaces. They overcome the sharp corners of branches and elbows. The movement of this robot was proportional to an Omni-directional versatile robot when guiding at corners.

4) Propellers for liquid mode configuration.

A propeller is a sort of fan that transmits power by changing over rotational movement into push. A weight contrast is delivered between the forward and raise surfaces of the airfoil-molded sharp edge, and a liquid, is quickened behind the cutting edge.

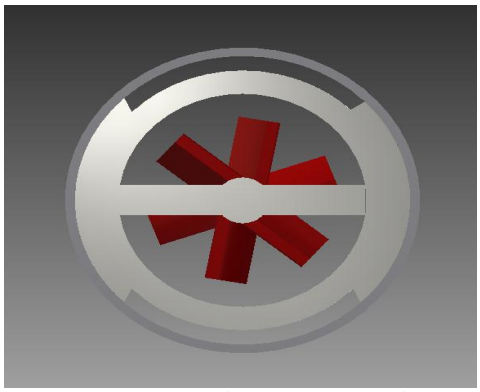

Fig: 2.2.7: Propeller for Liquid mode configuration

Propeller progression, similar to those of flying machine wings, can be created by either or both Bernoulli's rule and Newton's third law.

C. Design of fully assembled Robot.

As described earlier it is an amphibious robot, hence it should be capable of reconfiguration into two different modes. i.e. mode 1 and mode 2. For inspection of pipeline which transmits gases, robot is configured to mode 1 and if the medium is liquid then it is configured to mode 2. It can be easily configured without any skills as because the steps for re-configuring are very easy.

1) Gas configuraion .

In mode 1 configuration three arms are attached to the central body by means of screw at three different sides. Each arm have a caterpillar wheels and in order to maintain stability in movements suspensions are also additionally added to the robot arm. The full assembled robot is shown in the figure 2.3.1

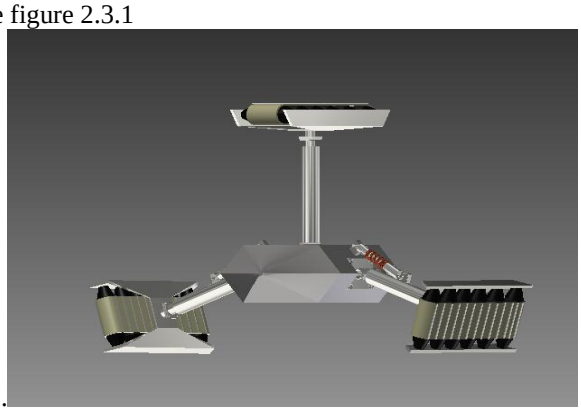

Fig 2.3.1: Robot in mode 1.

The front view of the robot is also shown in the figure 2.3.2. And its kinematic equations and motion planning are elaborated in section 3 and section 4.

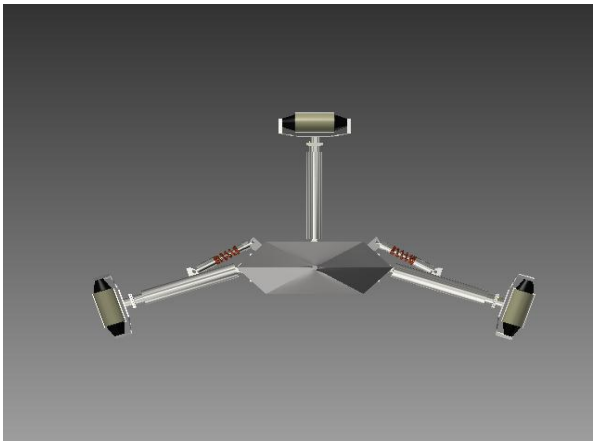

Fig 2.3.2: Robot in mode 1.

2) Liquid configuration.

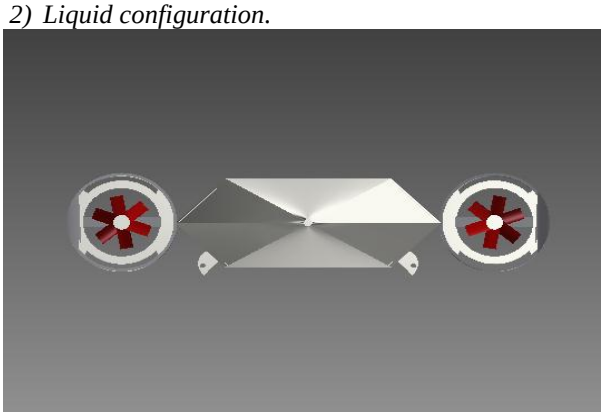

Fig 2.3.2: Robot in mode 2.

In mode 2 configuration three arms are detached from the central body by un-screwing. Now two propellers are added at same place where the arms are kept and these two propellers are fixed to central body by means of screw. Now it can be able to explore in liquid environment. The full assembled robot in mode 2 is shown in the figure 2.3.2.

International Journal of Engineering Research & Technology (IJERT)
ISSN: 2278-0181
Vol. 6 Issue 07, July - 2017

III. KINEMATIC EQUATIONS OF ROBOT

A. *Kinematic equations of robot in mode gaseous configuration mode.*

1) Overcoming gravity

The base typical power required for the robot to defeat gravity is

$$N \min = mg/2\mu$$

The robot have to travel in both vertical and horizontal axis of the pipeline hence, the force required for it to move will changes with change in axis and in order to travel in a stable state, it should first overcome its own body weight i.e it should overcome gravity

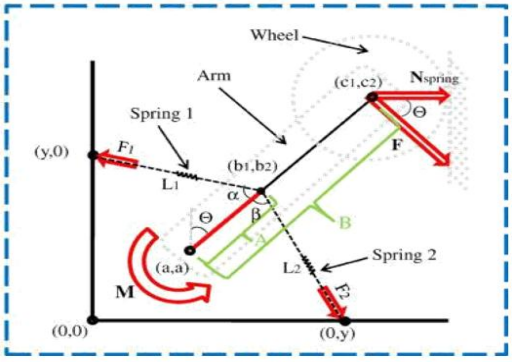

Fig 3.1.1: Free body diagram of robot arm.

μ and g are the coefficient of grinding and the speeding up of gravity, individually. To affirm with the parameters set to those could apply a power higger than the base power required, determined a condition for the ordinary power applied by the two springs (N spring).

$$X_{d1} = L_1 - X_1 \quad (1)$$

$$X_{d2} = L_2 - X_2 \quad (2)$$

$$b_1 = a + A \text{ transgression } \Theta \quad (3)$$

$$b_2 = a + A \cos \Theta \quad (4)$$

$$L_1 = \sqrt{b1+(y-b_2)^2} \quad (5)$$

$$L_2 = \sqrt{(y-b_2)2+b2^2} \quad (6)$$

$$\alpha = \cos^{-1}((A^2 + L_1^2) - (y-a)^2 - a^2/2L_1A) \quad (7)$$

$$\beta = \cos^{-1}((A^2 + L_2^2) - (y-a)^2 - a^2/2L_2A) \quad (8)$$

x_{d1}, x_{d2}, and x_i signify the prolonged lengths of spring 1 and spring 2 and the underlying length of the spring. On the off chance that x_{d1} or x_{d2} gets to be shorter than zero, the quality ought to be set to zero, in fact that the springs apply no power on the arm in these cases. The conditions for the minute on the pivot (an, an) applied by two springs and the typical power created by the springs.

$$M = kA(X_{d2}\sin\beta - X_{d1}\sin\alpha) \quad (9)$$

$$N \text{ spring} = F\cos\theta = M/B\cos\theta \quad (10)$$

The above equation gives the relationship between the N normal force and mass M and the angle θ, hence in order to overcome gravity the necessary variable are substituted and the required N will be sorted out.

2) Maximum torque required to move forward by overcoming moment.

The suspensions which are attached to robot arms will push the wheels towards the surface with high force, thus avoiding slipping and giving necessary traction force but in order to move forward the wheels must produce more torque than the moment created by arms suspension.

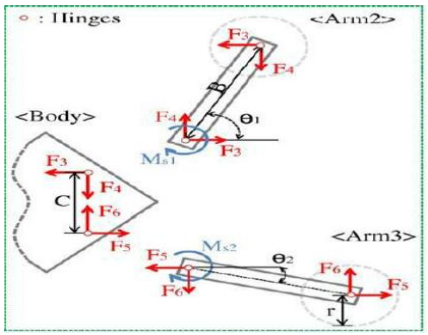

Fig 3.1.2: overcoming moment generated by springs

$$F_4 = F_6$$
$$F_3 = F_5 = T/r$$

A steady larger suspension spring constant increases the performance whereas, a smaller spring constant helps it to traverse a larger range of branch sizes. This indicates that modulating the spring constant can cause changes in its performance.

3) Kinemtaic equations of motion for robot.

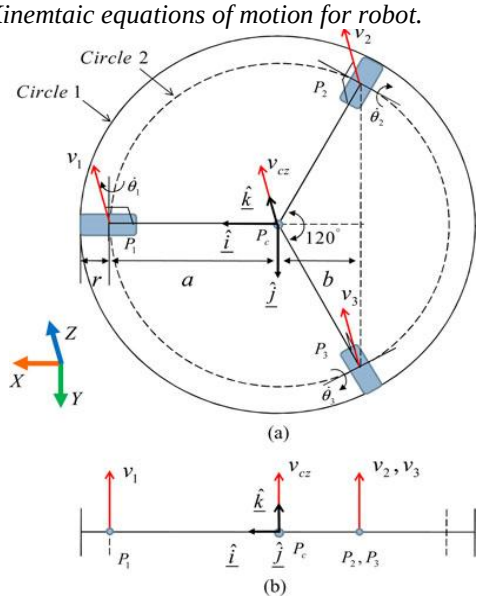

Fig 3.1.3: (a) Cross-sectional view of the pipeline. (b) Velocity profile at the side view of the pipeline.

$$v_2 = r\dot{\theta}_2 \quad (11)$$

$$v_3 = r\dot{\theta}_3. \quad (12)$$

To begin with, we expect that each caterpillar wheel holds a line contact at the internal mass of the pipeline, and that the wheel does not slip in the even course and does not turn about the z-hub, but rather is permitted to move along the z-pivot. The power created by the mounted micro-motor is transmitted to the caterpillar wheel through a slant gear. We characterize θ_1, θ_2, and θ_3 as the pivoting points of the caterpillar wheels; r indicates the sweep of the wheel, and a means the range of the

International Journal of Engineering Research & Technology (IJERT)
ISSN: 2278-0181
Vol. 6 Issue 07, July - 2017

robot body. At that point, the straight speeds v_1, v_2, and v_3 at the focal point of the wheels are given by

$$v_1 = r\dot{\theta}_1$$

The straight speeds v_1, v_2, and v_3 have diverse magnitude of velocities at elbows or T-branches. At that point, the straight speed at the middle Pc of the robot is signified as v_{cz} , and the rotational speeds about the body is $\hat{i}$ and $\hat{j}$ are meant as ω_x and ω_y . At that point, so as to infer the kinematic relationship between the information speed ($\dot{\theta}_1$, $\dot{\theta}_2$, and $\dot{\theta}_3$) and the yield speed (ω_x, ω_y , and v_{cz}), we break down the parts of the yield speed for four cases. Fig. 3.3.1 (a) and (b) demonstrates the cross-sectional perspective of the pipeline and the speed profile along the edge perspective of the pipeline, individually.

Case 1 ($v_1 = v_2 = v_3$): Case 1 is the state in which the robot moves in the straight pipeline. As appeared in Fig.3.3.1: (a), the three wheels speeds are equivalent; consequently, the direct speed v_{cz} at the middle can be depicted as

$$v_{cz} = v_1 (= v_2 = v_3) \quad (13)$$

The rotational velocities ω_x and ω_y didn't exist.

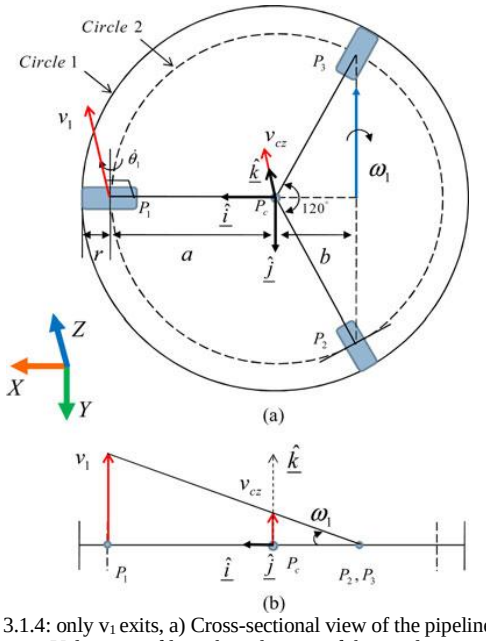

Fig 3.1.4: only v_1 exits, a) Cross-sectional view of the pipeline. (b) Velocity profile at the side view of the pipeline

Case 2 (Only One Velocity Exists (v1): case 2 is the state where one and only speed exists, For this situation, the focuses P_2 and P_3 are stationary, and at the point P1, a direct speed v_1 is produced. At that point, the straight speed at the middle Pc of the robot is acquired by geometric investigation. Resultantly, the robot pivots about the line P_2, P_3 with the rotational speed ω_1 given by the following equations

$$\omega_1 = v_1 /(a + b) \quad (14)$$

Since $b = a \cos 60°$, (3) becomes

$$\omega_1 = v_1/(1.5)a \quad (15)$$

The straight speed v1 is created by turn of the caterpillar wheel,which can be written as

$$v_1 = r\dot{\theta}_1 \quad (16)$$

The rotational velocity vector ω_1 with respect to the local co-ordinate of the robot can been written as

$$\omega_1 = -\, r/(1.5a)\, \dot{\theta}_1 \quad (17)$$

The rectilinear components of ω_1 can be written as

$$\omega_x = 0 \quad (18)$$

$$\omega_y = -\, r/(1.5a)\theta_1 \quad (19)$$

Linear velocity v_{cz} at the center of the robot is

$$vcz = b/(a + b) = v_1 = 0.5a/(1.5a)v_1 = r3\dot{\theta}_1 \quad (20)$$

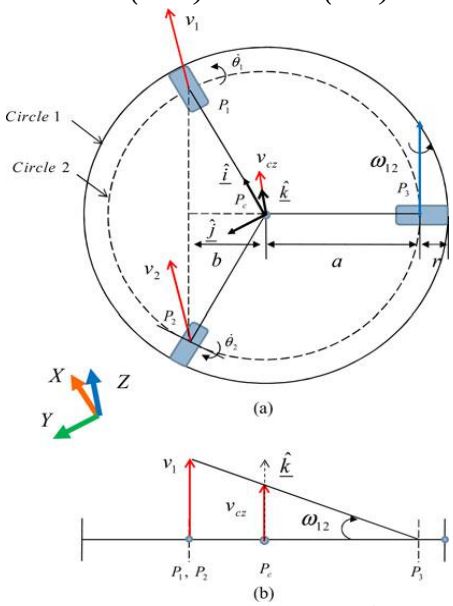

Fig 3.1.5: V_1 & V_2 exits, a) Cross-sectional view of the pipeline. (b) Velocity profile at the side view of the pipeline

Case 3 (Two Velocities Exist (v_1, v_2)): Case 3 is the state in which two speeds exist, For this situation, the point P_3 is stationary, and at the points P_1 and P_2 , the straight speeds v_1 and v_2 are created. At that point, the direct speed at the middle Pc of the robot is gotten by geometric investigation. Resultantly, the turn speed ω_{12} is created by the straight speed v_1 and v_2 .when the direct speeds v_1 and v_2 are the same, the rotational speed ω_{12} is given by

$$\omega_{12} = v_1/(a + b) = v_1/(1.5a) \quad (21)$$

The rotational velocity vector $\omega 12$

$$\omega_{12} = r\theta_2/(\, 1.5a(\cos 30° \hat{i} - \sin 30° \hat{j}))$$

$$\omega_{12} = \sqrt{(3r/3a)\theta_2}\hat{i} - r3a\dot{\theta}2\hat{j} \quad (22)$$

$$v_{cz} = a/(a + b)v_1 = a/(1.5a)v_1 = 2r/3(\theta_1) \text{ or } 2r/3(\theta_2) \quad (23)$$

Case 4 (v1 = v2 = v3): Case 4 is the state where three speeds exist together with various qualities (e.g., $v_3 < v_2 < v_1$). For this situation, the rotational speed vector of the robot is equivalent to the summation of the rotational speed vector made by the straight speed of every wheel. That is to say, when just v_1 exists, the rotational speed vector is indistinguishable to (19). Additionally, when just v_2 exists, the rotational speed vector is as per the following:

$$\omega_2 = r\dot{\theta}_2/1.5a\ (\cos 30° \hat{i} + \sin 30° \hat{j})$$
$$= \sqrt{3r/3a(\dot{\theta}_2}\hat{i}) + r/3a(\dot{\theta}_2\, \hat{j},) \quad (24)$$

International Journal of Engineering Research & Technology (IJERT)
ISSN: 2278-0181
Vol. 6 Issue 07, July - 2017

Where $\omega_x = (\sqrt{3}r/3a)\dot{\theta}_2$, and $\omega_y = (r/3a)\dot{\theta}_2$.

$$\omega_2 = r\dot{\theta}_3/1.5a\,(-\cos 30^\circ \hat{i} + \sin 30^\circ \hat{j}) = -\sqrt{3}r/3a\dot{\theta}_3\hat{i} + r/3a\dot{\theta}_3\hat{j}, \quad (25)$$

Where $\omega_x = -(\sqrt{3}r/3a)\dot{\theta}_3$, and $\omega_y = (r/3a)\dot{\theta}_3$.
Assuming that v_1, v_2, and v_3 exist at the same time,

$$\omega = \omega x\hat{i} + \omega y\hat{j} \quad (26)$$

$$\omega x = \sqrt{3}r/3a(\dot{\theta}_2) - \sqrt{3}r/3a(\dot{\theta}_3) \quad (27)$$

$$\omega y = -(2r/3a)\dot{\theta}_1 + (r/3a)\dot{\theta}_2 + (r/3a)\dot{\theta}_3 \quad . (28)$$

The velocity v_{cz} at the center of the robot is given as

$$v_{cz} = 1/3(v_1 + v_2 + v_3) = r/3(\dot{\theta}_1 + \dot{\theta}_2 + \dot{\theta}_3) \quad (29)$$

Finally, the relationship between the input velocity vectors which are obtained is as follows
$\dot{\theta}_a = (\dot{\theta}_1\,\dot{\theta}_2\,\dot{\theta}_3)^T$ and the output velocity vector
$\dot{u} = (\omega_x\,\omega_y\,v_{cz})^T$ is constructed as

$$\dot{u} = [G_{ua}]\,\dot{\theta}_a \quad (30)$$

Combining (15) and (18). Here, the Jacobian is given as

$$[G_{ua}] = \begin{matrix} 0 & \sqrt{3}r/3a & -\sqrt{3}r/3a \\ -2r/3a & r/3a & r/3a \\ r/3 & r/3 & r/3 \end{matrix} \quad (31)$$

For a given direct speed (vcz) and rotational speeds (ωx and ωy) at the focal point of the robot, the precise speed of the wheels are computed as

$$\dot{\theta}_a = [G_{ua}]^{-1}\,\dot{u}. \quad (32)$$

The pivot angle of every wheel is obtained by numerical integration of (32).

B. Kinematic equations of robot in mode 2(liquid configuration)

Travelling in a live stream tunnel is hard for a robot. A tunnel is a bound domain. The stream inside this channel cooperates with the robot and it might make unsettling influences on the robot. The liquid field at a Tee intersection can be exceptionally turbulent, and its impacts on the swimming movement of the robot have not been concentrated adequately previously. The robot must have precise control framework so it can move securely in the tunnels. Those difficulties can be overcomed. A legitimate shape outline can permit the swimming robot to defeat the liquid aggravations. A legitimately composed robot can move inside a liquid stream effortlessly. It can likewise exploit the liquid field at Tee intersections to recognize the Tee intersection and additionally perform turns. Swimming robots perform moves all the more dependably and productively.

1) Notations and parameters

This robot have six degrees of freedom and the notions used in this section are briefed in the Figure 3.2.2.

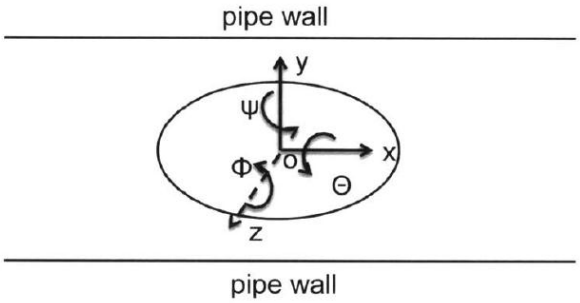

Fig 3.2.1: body fixed reference frame

x, y, z are the direct positions, and u, v, w, are their relating straight speeds. *Θ, ω,* are the angular position about x, **y,** *z* axes as showed in Figure 3.2.1.

position	velocity	angular position	angular velocity
x	$\frac{dx}{dt} = u$	θ	$\frac{d\theta}{dt} = p$
y	$\frac{dy}{dt} = v$	ψ	$\frac{d\psi}{dt} = q$
z	$\frac{dz}{dt} = w$	ϕ	$\frac{d\phi}{dt} = r$

Figure 3.2.2: Notations used to describe the robot hydrodynamics.

It is assumed that the robot is neutrally buoyant so the gravity and buoyancy forces cancel each other out in the z direction. To study the motion in the xy plane only, all out of plane variables can be assumed to be zero.

$$z = 0, w = 0, 0 = 0, V) = O, p = 0, q = 0 \quad (33)$$

2) Low axial drag force

The first challenge is the fluid drag force. The drag force makes it difficult for the robot to maneuver in and opposite to the direction of the flow and thus should be kept low. In general, drag force, *FD*, is defined as follows.

$$FD \sim 1/2\,(pC_DA_oU_r^2) \quad (34)$$

where p is the fluid density, CD is the drag coefficient, AO is the projected area of the robot in the direction of the flow and ***U,*** is the relative velocity between the fluid and the robot. Equation (34) is for open water only. CD is a dependent on the robot's shape and the confined environment. Shapes such as ellipsoids have low drag coefficients. A swimming robot experiences a large drag force in a confined environment than in an open fluid medium. The fluid is confined between the pipe wall and the robot. This phenomenon puts a hard cap on the size of the robot. Smaller AO can be achieved by reducing the overall size of the robot or adjusting the robot's cross-section profile.

3) Design for angular and radial stability.

The second challenge is the angular stability and radial stability. As shown in Figure 3.2.2. when the x axis of a robot is not aligned with the flow, or it is at a nonzero angular offset **(a),** it will experience some drag, lift and Munk moment. There is always a drag force when the robot is moving in a fluid. The Munk moment (M) occurs due to the unevenly distributed fluid pressure on the robot, and it is zero on axial symmetric shapes. The Munk moment can be calculated as follows.

International Journal of Engineering Research & Technology (IJERT)
ISSN: 2278-0181
Vol. 6 Issue 07, July - 2017

$$M = 1/2(\text{Ayy} - Azz)U_2 \sin(2a) \quad (35)$$

Where AYY and A**.,** are the added mass in the **y** direction and the added mass in the x direction, respectively. For shapes that have the same profile in the x and **y** directions, **A,,** will be equivalent to AYY**.** Thus the Munk moment is zero.

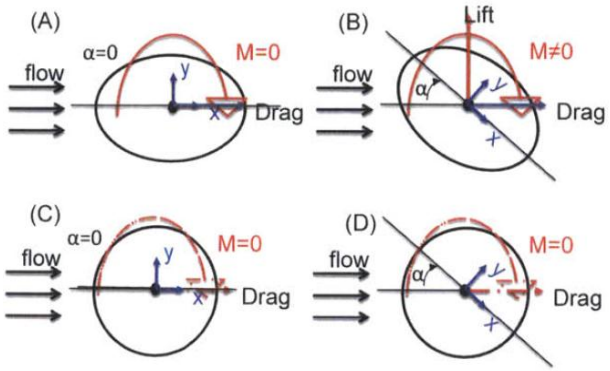

Fig 3.2.2: Fluid forces and moments on different shapes at different angular offset.**(A)** and (B): a robot with different profiles in x and **y** direction experiences a Munk moment **(C)** and **(D):** a robot with the same profile in x and **y** direction experiences no Munk moment.

The difference in static pressure on each side of the robot will drive the robot to the side with smaller opening and eventually it hit the pipe wall. This destabilizing force is the basis of Venturi's Effect. It increases with ***dy*** as well as the relative velocity between the fluid and the robot, and it has a tendency to force the robot to move away from the centerline of the pipe.

The answer for reducing drag power is to put ducts through the robot with aerodynamically body as shown in Fig 3.2.3. Rather than circumventing the robot, the liquid can experience the conduits. The second technique is to keep up a low relative speed with the stream. The Venturi's Effect is then minimal, and the robot can easily correct its heading direction.

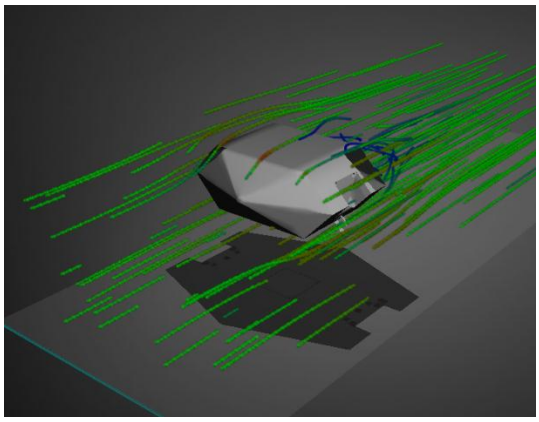

Fig 3.2.3: Fluid forces and moments on different shapes at different angles.

4) Equations for minimal turning radius and yaw controlling.

The shape of the robot can be designed for minimum turning radius through the study of the first order approximation of the hydrodynamic forces. The hydrodynamic force about the geometric center of the robot in the x direction can be expressed as [4] **X(X,** y **z, U, V,** ***W, p, q,*** *r,* i..,.,). The same can be applied to hydrodynamic force in the **y** direction, Y, and hydrodynamic moment about the z axis, ***N.*** Since we assume the robot motion is confined to the horizontal plane, hydrodynamic forces and moments that are out of the horizontal plane can be assume to be zero. This is the case if the robot is properly balanced and the flow in the pipe is not rotating.

The hydrodynamic forces are the net forces on the robot. The momentum principle says the change of momentum is equal to the net force:

$$X = m[ih + qw - rv + 4ZG - yG + (qyG + rZG)p - (\boldsymbol{q}^2 + r^2)xG] \quad (36)$$

$$\boldsymbol{Y} = m[b + ru - pw + rXG - PZG + (rzG + pxG)p - (r^2 + \boldsymbol{p}^2)YG] \quad \textbf{(37)}$$

$$\boldsymbol{N} = IzxP + Izy4 + Izzr + (Iyy - Jxx)pq + Ixy(p\,2 - \boldsymbol{q2}) + Iyzpr - Ixzqr + m[xG\,() + \boldsymbol{ru} - pw) - YG(it + qw - rv) \quad (38)$$

where *m* is the mass of the robot. x, **y,** *z* are defined as small position deviations from the zero position in the x, **y,** z directions. *it* is the linear acceleration in the x direction) is defined as the time derivative of *u* (linear speed in the x direction). *XG, YG, ZG* is the position of the center of mass with respect to the center of the geometry. *Iz, Iy,, Iz,* are the moment of inertia about x, **y** and z axes. Ixy is the coupling between different axes. The hydrodynamic forces can be linearized following the **method described above.** The first order approximation of the hydrodynamic force X can be calculated as follows.

$$X = Xxx + Xyy + Xzz + XoO + XpO + XOb + Xu + Xv + Xw + Xp + Xq + Xr + Xit + Xbi + \boldsymbol{Xjbh} + \boldsymbol{Xpp} + X44 + Xtt + \boldsymbol{...} \quad (39)$$

Force *Y* and moment ***N*** can be calculated with Equations (40) and (41).

$$Y = Yx + \text{YY} + \text{Yzz} + Yo + \text{Yp} + \text{Y,6} + \text{Yu} + Yv + Yu + Y\sim p + Yqq + \text{Yr} + \text{Ya} + Yi) + Yob + YpP + Y44 + Y\,. \quad (40)$$

$$\boldsymbol{N} = Nxx + Nyy + Nz\,z + NoO + N + No + Nuu + Nv + Nw + Npp + Nqq + Nrr + Nit + \boldsymbol{Nbi} + \boldsymbol{Nbs} + NpP + N44 + N4 + ... \quad (41)$$

Including input forces and moments, the hydrodynamic equations then become as follows.

$$X = Xuu + Xev + Xrr + Xa6 + \boldsymbol{X,}) + Xtt + \text{Xzput} \quad (42)$$

$$\text{Y} = \text{Yy} + Yu + \text{YV} + \text{Y,.r} + Yj + yoh + \text{Y} + \text{Yinput} \quad (43)$$

$$\boldsymbol{N} = Nuu + Nov + Nrr + Na6 + Nb + i) + \boldsymbol{N} + \text{Ninput} \quad (44)$$

Where Xinpt Yinput and Ninpt represent the input forces and moment generated. the momentum equations become

$$\boldsymbol{X} = m[it - rv - TYG + rxG] \quad (45)$$

$$Y = m[i + ru + rxG - r2YG] \quad (46)$$

$$\boldsymbol{N} = \text{Izzi} + m[xG(Lb + ru) - YG(\boldsymbol{U} - rv)] \quad (47)$$

International Journal of Engineering Research & Technology (IJERT)
ISSN: 2278-0181
Vol. 6 Issue 07, July - 2017

If the robot has multiple planes of symmetry like a circular plate or a sphere, any motion in the x direction will not result in hydrodynamic forces in the y direction or torque in yaw direction. The same thing applies to motion in the y direction and rotating in the xy plane. Therefore Xv, Xr, Xe,, X, Y&, Ye, Nu,No, N, Ni, are all zero when the robot have the same symmetric profiles in xy, yz and xz planes. Furthermore, the added mass in yaw direction N can be approximated zero if the robot has a circular profile in the horizontal plane.
The coupling among different axes can be further reduced. These two centers should at least be the same in the XY plane, thus ***XG = 0, YG = 0.*** Then the hydrodynamic equations and momentum equations for a robot with the same symmetric profiles in xy, yz and xz planes are expressed as follows.

$$X = m(ii - rv) = \text{Xuu} + Xuit + \text{Xinput} \quad (48)$$
$$Y = m(b + \text{ru}) = \text{Yyy} + \text{Yv} + Y + \text{Yinput} \quad (49)$$
$$N = Izzi = Nrr + \text{Nznput} \quad (50)$$

IV. MOTION PLANNING.

Few analyses were done to check movement ability of the robot at 45 and 90 degrees elbows, Tee, and Y-branches. At 45 and 90 degrees elbow, there are 3 sorts, at T-branch, there are 16 sorts, and at Y-branch, there are 22 sorts of movements. Distinctive sorts of robot movement in various pipeline twists 45 and 90 degrees elbows, T-, and Y-branches) are shown in fig 5.1 below.

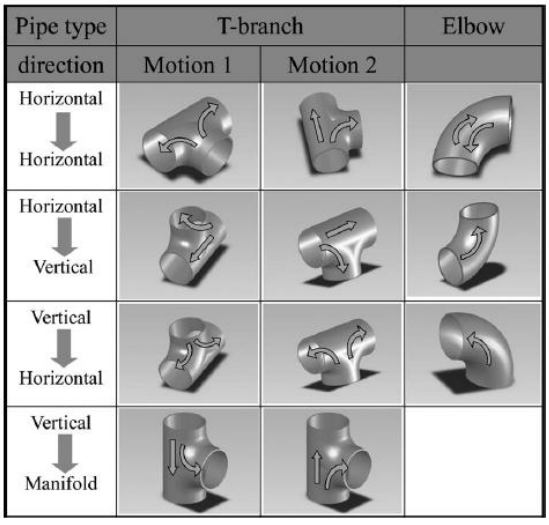

Fig 4.1.1: Different motions in elbow & T -branches.

A. *Motion planning of robot in mode 1(gas configuration).*

1) Motion planning 45 degrees elbow.

The movement arranging of the robot at 45 degrees elbow is like the movement arranging of 90 degrees elbow given beneath.

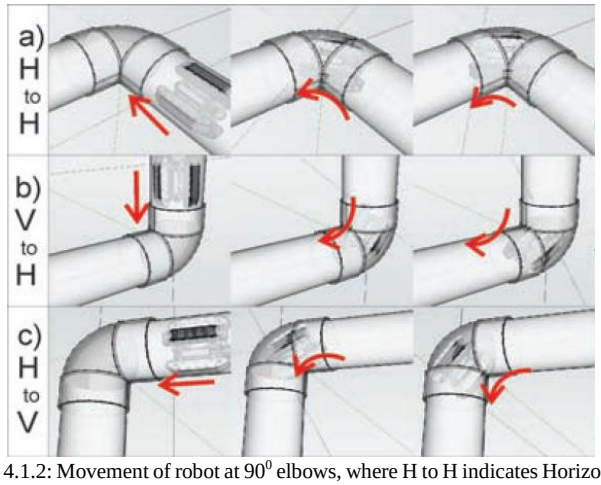

Fig 4.1.2: Movement of robot at 90^0 elbows, where H to H indicates Horizontal to Horizontal, V to H indicates Vertical to Horizontal, and H to V indicates Horizontal to Vertical motion.

2) Motion planning at 90 degrees elbow and T-branch.

The movement arranging of the robot at 90 degree elbow is given in Fig. 4.1.2. The robot make a turn by making stationary the wheels reaching the internal corner of the 90 degrees elbow and pivoting the wheels reaching the external side of the 90 degrees elbow toward vertical or even heading it expects to turn.
The motion of the robot at T-branch is given in Fig.4.1.3 it has been seen that movement arranging at T-branch is more difficult because there are numerous ways at the T-junction. The turning from flat to the vertical axis inside the pipeline is difficult. This is because of the low contact for the caterpillar wheels to have the capacity to reach to within limits of the pipeline.

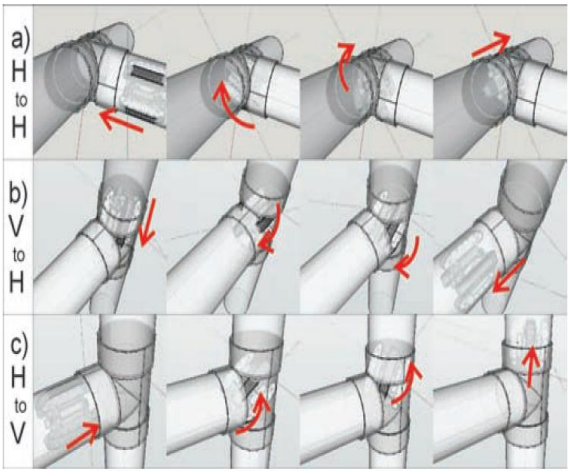

Fig 4.1.3: motion planning of robot at elbow

B. *Motion planning of robot in mode 2(liquid configuration).*

1) Moving in straight line and in a 45 degree elbow.

Motion planning is same for straight and 45 degree elbow in pipeline as because the liquid stream in pipe automatically adjusts the robot motion, if only the robot body is suitably designed with necessary considerations. The simulation set up is shown in Figure 4.2.1. The robot is put stationary at the focal point of a round tunnel of distance across D and length 2LP. The ducts of the robot are adjusted to the course of the stream. The liquid streams from the channel to the outlet. At the inlet

International Journal of Engineering Research & Technology (IJERT)
ISSN: 2278-0181
Vol. 6 Issue 07, July - 2017

the stream is accepted to have a uniform speed U. Since the robot is stationary, the relative speed between the robot and the liquid, U_o = U. The relative movement, between the robot and the liquid stream, results in a liquid drag power FD on the robot. The objective of this reproduction is to locate the most extreme estimation of FD for every single craved move.

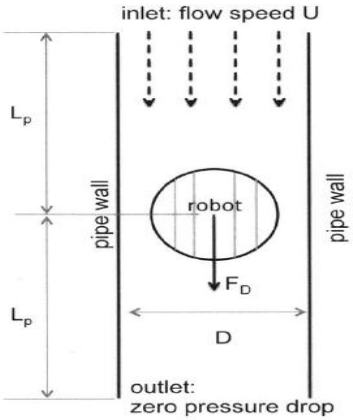

Fig 4.2.1: Motion of robot in straight pipe line

At the point when the robot is moving in a straight pipe, it ought to buoy, brake or keep up a stationary position. The majority of the wanted moves are toward the liquid, as showed in Figure 4.2.1. The liquid drag power scales with the square of the relative speed. The relative speed and FD are the biggest when the robot is stationary.

Table 4.1
Parameters used in cfd simulation

Parameters	value
Pipe Diameter D	100 mm
Flow speed U	1 m/s
Distance L	4 m
Reynolds's number Re	100,000

The CFD simulation predicts FD in the axial direction of 0.722 N. This drag force tries to push the robot toward the outlet. It is the main huge hydrodynamic force in this situation, and it is more than 100 times greater than the liquid force which is acting in radial direction. The close-up horizontal cross section view of the simulation is shown in Figure 4.2.2. In this figure, the liquid streams into the channel from the top. The stream before the robot has a normal speed of 1 m/s. It boosts to a velocity of 2.135 m/s when it is moving in the pipe.

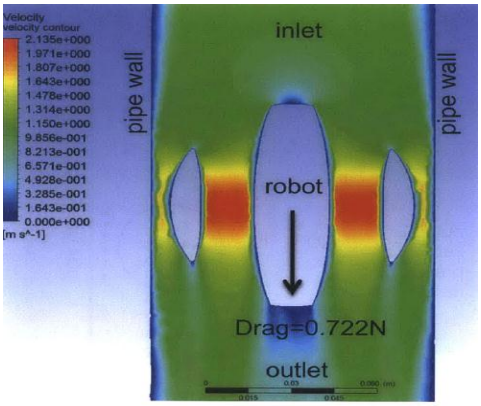

Fig 4.2.2: Horizontal cross-section view of the simulated robot placed in the fluid.

2) Turning at A Tee Junction.

A second CFD recreation is performed to locate the liquid forces on the robot when it is turning at a Tee intersection. The recreated situation is shown in Figure 4.2.3. The Tee intersection associates three straight pipe areas of breadth D and length Lp. The robot is situated in the focal point of the Tee intersection at the moment of a turn. It is observed that a liquid stream of uniform speed U enters the inlet. The liquid then split into two streams, one streaming towards the outlet 1 and the other to outlet 2. The conduits of the robot are adjusted to the course of the stream at the channel. The robot encounters axial force FD and a side force Fs. The objective of this simulation is to find out the values of these two forces. For consistency with the straight pipe situation, the same parameters in Tables 4.1 are utilized as a part of this simulation.

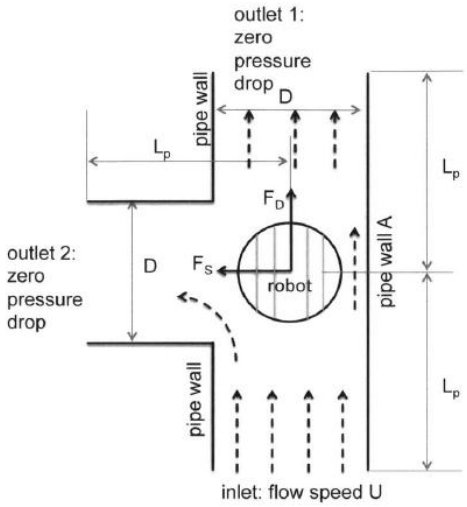

Fig 4.2.3: Cross-section view of the Tee junction and the robot in the simulation. The robot is placed at the center of the Tee junction.

Assumption is that the two outlets have the same pressure. The fluid is driven by its momentum instead of pressure difference. It is expected that more flow is going straight to outlet 1 than turning into outlet 2.

The CFD simulation predicts a switched drag force. A nearby up perspective of the stream field as far as speed vectors is appeared in Figure 4.2.4. The drag power is - 0.282 N, so it is pushing the robot up-stream toward the inlet. . As appeared in Figure 4.2.5, the liquid stream extends and the stream speed

International Journal of Engineering Research & Technology (IJERT)
ISSN: 2278-0181
Vol. 6 Issue 07, July - 2017

decreases as the liquid enters the Tee intersection. The stream speed U decreases because of the conservation of mass, and hence the static pressure increase. At area B in Figure 4.2.5, the stream velocity is higher and the static pressure is lower than that at area C. This static pressure difference will push the robot to move toward area B or toward the inlet. This opposite drag force can help the robot to moderate down when it touches base at a Tee intersection.

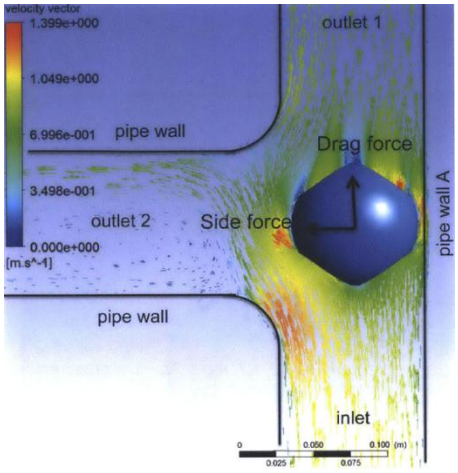

Fig 4.2.4: Flow visualization for the robot inside a Tee junction. ***FD*** and force *Fs* are measured**.**

The CFD simulation also predicts a Venturi's force. The side force on the robot is predicted to be -0.337 N**.** This side force consists mainly of the Venturi's force which always pull the robot closer to pipe wall A and consequently prevents the robot from moving toward outlet 2. Since the reversed drag force helps the robot slow down, the robot can take advantage of it during maneuvers at the Tee junction. A robot needs to overcome the radial force of at least 0.337 N in order to make it to the side pipe. Thus by applying of 0.337 N of force it can move into the side of tee junction. The side force changed as the robot was turning but it maintained its direction. The Venturi's effect kept attracting the robot to the wall and prevented it from entering the side pipe for all robot's possible angular positions. The robot mustbe able to overcome this Venturi's effect in order to move into the side pipe.

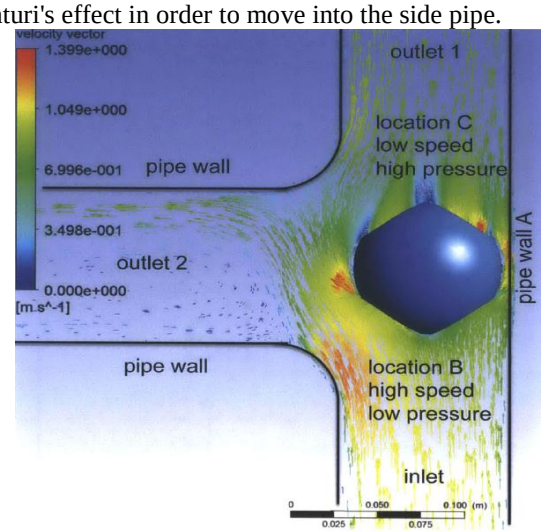

Fig 4.2.5: Flow visualization for the robot inside a Tee junction. Location B has higher flow speed and lower static pressure than location C**.**

The same CFD simulation were performed for the robot at different angular position in order to find how the fluid forces are changed. The results show that the drag force changes significantly during the turn. The results are plotted in Figure 4.2.6

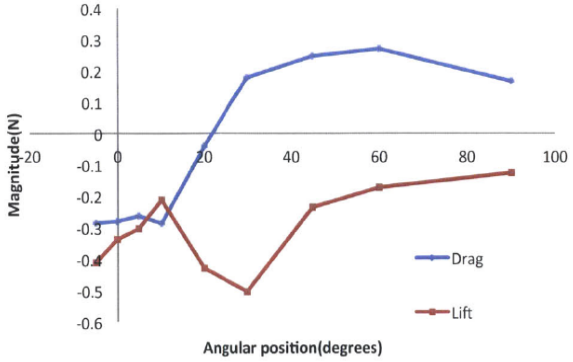

Fig 4.2.6: Simulated force on the improved robot at different angular positions.

V. SENSORS CONFIGURATION.

A. Installation of BMP180 shield.

In order to measure the pressure, temperature and humidity in pipes, robot requires a compatible sensors and microcontroller configuration. The microcontroller have to program correctly for ensuring the correct working.

Despite using 3 different sensors for measuring pressure temperature and humidity, only one shield (bmp180) is used to measure all three variables. And microcontroller which is used is Aurdino Uno, with proper program code and proper pin alignment it will run effectively and efficiently.

Configuration of BMP shield with aurdino is showed in the Figure 5.1.1 and its working condition BMP shield is connected to aurdino by means of data transmission wires

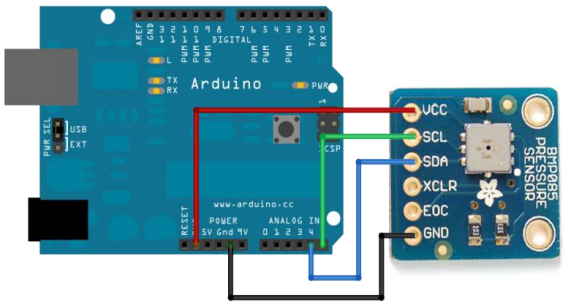

Fig 5.1.1: Configuration of aurdino bmp 180 shield

These values are transferred to control room for further analysis.

B. Installation of Gps

Gps is the major sensor when compared to rest of the other sensors, because without gps co-ordinates, it cannot find out exact location of the leak. Then these co-ordinates are transferred to control system then the welding team will be sent to the exact location where leaked observed.

International Journal of Engineering Research & Technology (IJERT)
ISSN: 2278-0181
Vol. 6 Issue 07, July - 2017

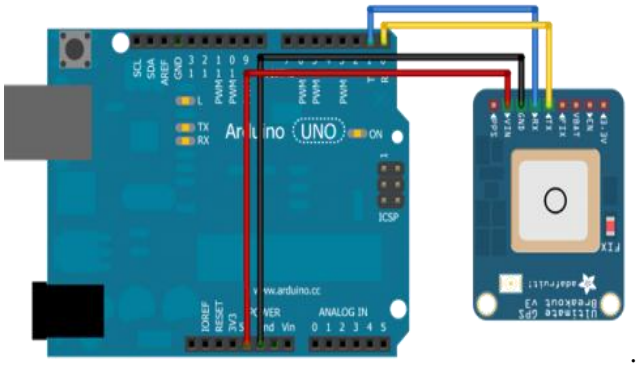

Fig 5.2.1: configuration of aurdino gps shield.

Configuration of gps shield with aurdino is showed in the Figure 5.2.1 and its working condition the gps shield is connected to aurdino by means of data transmission wires [5]..

VI. IMPLEMENTATION.

The parts of the robot are little, yet effective processing framework based on Gumstix primary board is helped by two interface sheets: robostix and wifi-stix [6]. They are interconnected to all the inner ports of the Gumstix, Robostix, and WiFi-stix, and additionally with the connected sensors and outside controllers. They additionally manage the force for all the interior sheets. This design gives simple and all inclusive access to every one of the ports accessible in front and back part of the central body.

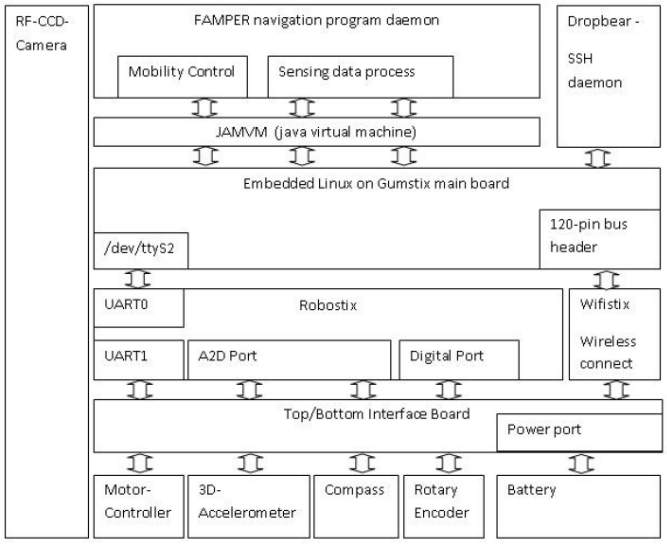

Fig 6.1: Electronic architecture for mode 1

Figure 6.1 demonstrates the schematic chart of the robot equipment in mode 1. The robot has connected RF-CCD Camera, which can send the video-stream autonomously the sensors, a 3Daccelerometer, a compass, and a turning encoder for specific purposes. Robostix gives the obliged pins to peruse information from accessible sensors by sending them to the Gumstix after converting them from analog to digital. WIFI-Stix includes the usefulness of transmitting and accepting information to and from a remote PC utilizing remote system. Gumstix is introduced with implanted Linux stage which has the capacity of running projects composed on abnormal state dialects. In this execution, we customized the controlling interface utilizing Java. The sensor readings have been perused utilizing programs written in AVR-C which are later ported to the Robostix.

Figure 6.2 demonstrates the schematic chart of the robot equipment in mode 2. In this chart, all arrows indicate the power transfer, while all dashed arrows indicate the data exchange. Beginning from the upper left, the batteries are associated straightforwardly to the two moor speed controllers. Each of them have the capacity to control the voltage and give a 5 V voltage supply to the Arduino smaller scale controllers. The first micro controller operates on a 5 V logic level.

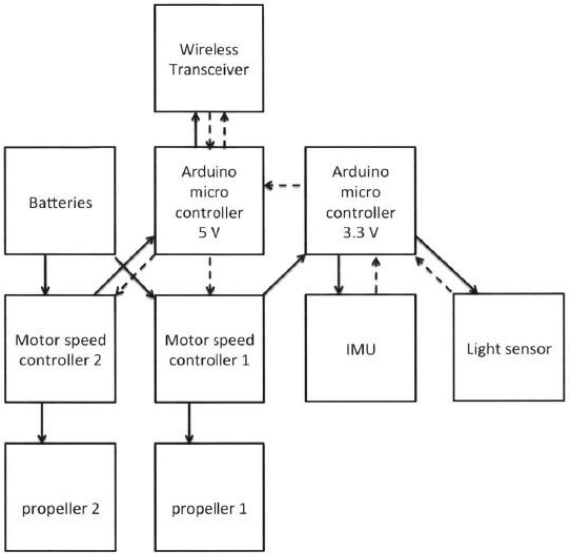

Fig 6.2: Electronic architecture for mode 2

It commands the wireless transceiver via serial communication and the two motor speed controllers via its digital output ports. The second Arduino small scale controller keeps running on a 3.3 V rationale level which is required by the IMU. This Arduino gathers and incorporates data from the IMU, light sensors before it sends data to the 5 V Arduino through Inter-Integrated Circuit (I2C) communication.

The 5 V Arduino then follows up on the data, makes new speed orders for the motor controllers and commands remote handset to report the robots status. The motor controllers, upon accepting the new orders, adjust their rotating speed to the propellers. It results in the propellers changing their turn speed and thrust output.

A. User inerface.

A Manual Control Program (MCP) has been created to work the robot in various pipeline formats. The system involves four noteworthy boards: (a) 3D perspective of the robot's position; (b) RF video board to show video stream from RF camera; (c) Control Panel (CP) to control the robot utilizing the robot Controller (FC) and/or the GUI interface and to give the tilting and course of the robot as demonstrated in little 3D perspective; and (d) Message Console (MC) to show the point by point status of the robot. The controlling signs are sent to the PC running the MCP utilizing FC as given as a part of Fig.

International Journal of Engineering Research & Technology (IJERT)
ISSN: 2278-0181
Vol. 6 Issue 07, July - 2017

6.3. FC utilizes a simple joystick furthermore gives adaptability of sending the control signals utilizing Bluetooth and USB associations. With a specific end goal to control the robot from a remote area, we utilized RF video framework which is little in size, devours low power, and have high affectability in assessing the circumstances inside the pipeline.

Robot is included with bright LEDs which help the RF camcorder framework to catch the robot environment.

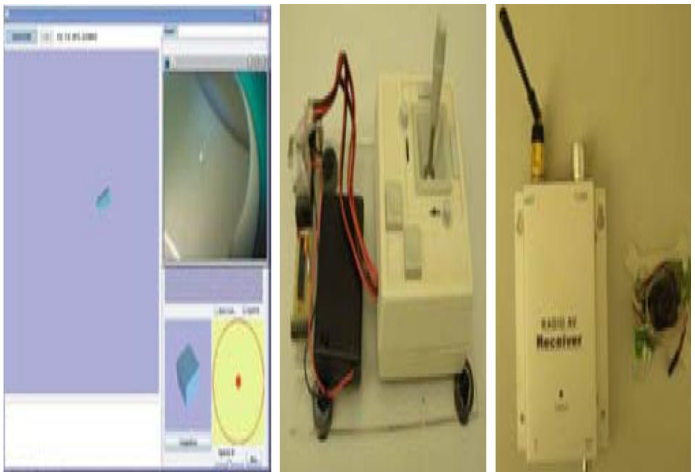

Fig 6.3: (a) Manual control program (b) FC Controller (c) RF video system

VII. EXPERIMENT.

The Prototype of scale 1:7 is prepared for testing the design and working capabilities. For the trial assessment, the robot is utilized in the examination of a complex pipeline design that has been developed utilizing all accessible pipeline fittings that a regular pipeline framework utilizes, where the robot additionally needs to perform vertical and even movement. Review that one of such complex pipeline format utilized as a part of the investigations is given in Fig. 4.1. The robot is initially tested in every curves separately and afterward tested to the entire pipeline format. The robot figures out how to go through the format by changing the servo motor speed suitably.

A. Motion at 90 elbow.

The Fig. 7.1 demonstrates that the pipeline inspection robot is heading out to numerous movements in several axis (moving up and down in the vertical pipeline) in the 90 degrees elbow of the trial pipeline format (movement at 45 degrees elbow is similar to 90 degrees).

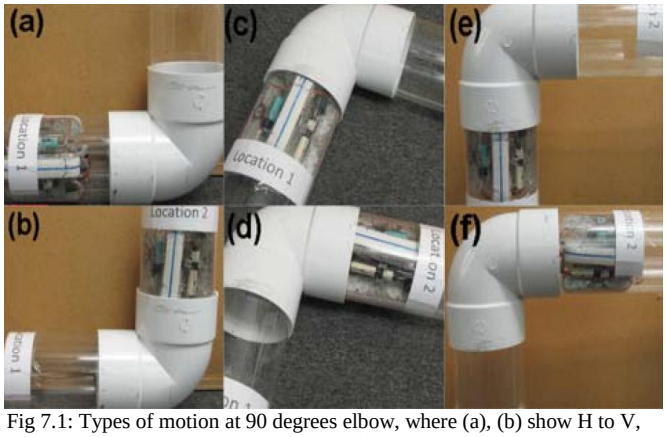

Fig 7.1: Types of motion at 90 degrees elbow, where (a), (b) show H to V, (c), (d) show H to H, and (e), (f) show V to H motion.

B. Motion at T-junction..

The Fig. 7.2 demonstrates that the robot setting out to a few turnings in a T-branch of the exploratory pipeline design. The movement of individual caterpillar wheels with different speed rate with programmed motion planning helps in maneuvering these complex pipeline geometry. Thus it proves that the design is compact and efficient.

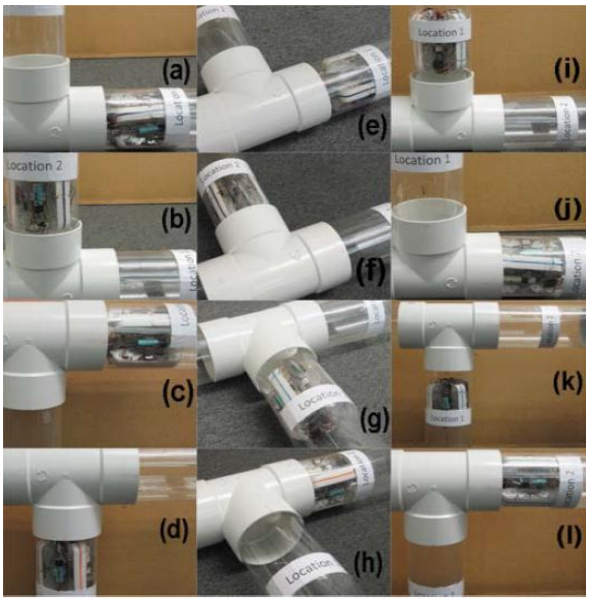

Fig 7.2: Types of motion at T-branch, where (a)-(d) show H to V, (e)-(h) show H to H, and (i)-(l) show V to H motion.

VIII. CONCLUSION

With the help of various experimental results, the design and movement planning of this robot is perfected. Thus it can be utilized for the detecting leakages in pipeline, exploration in sewage tunnels and other industrial pipe lines [7].

The designed pipeline inspection robot which is shown in figure 1.2.1 can inspect 30–36 Inch pipelines while this prototype is used to inspect the medium pipelines of sizes below 200 mm diameter. Robot module comprises of three sets of caterpillar wheel base, each of which is worked by a small dc motor. Free control of each Caterpillar wheels permits, directing ability through elbows or T-branches cross-sectional area.

International Journal of Engineering Research & Technology (IJERT)
ISSN: 2278-0181
Vol. 6 Issue 07, July - 2017

IX. ACKNOWLEDGMENT .

I wish to thank Hepsiba seeli, Sri Harsha Dorapudi, S Naveen kumar and other college Faculty member's along with our lab technicians.

X. REFERENCES.

[1] Oya and T. Okada, "Development of a steerable, wheel-type, in-piperobot and its path planning," *Adv. Robot.*, vol. 19, no. 6, pp. 635–650,2005.

[2] Pasala Venkata Satish, Sri Harsha Dorapudi, Hepsiba Seeli, Samanthula Naveen Kumar. (Volume. 6 - Issue. 03 , March - 2017) . " Design of an In-pipe Inspecion Robot ", International Journal of Engineering Research & Technology (IJERT) , ISSN: 2278-0181 , www.ijert.org,
DOI: http://dx.doi.org/10.17577/IJERTV6IS030121

[3] Transeth and K. Y. Pettersen, "Snake robot obstacle-aided locomotion: modeling, simulations, and experiments," *IEEE Trans. Robot.*,vol. 24, no. 1, pp. 88–104, Feb. 2008.

[4] Roth, K. Schiling, S. Futterknecht, U. Weigele, M. Risch, "Inspection and repair robots for waste water pipes, a challenge to sensories and locomotion", Proc. of IEEE International Conference on Robotics and Automation, pp. 476-478, 1998.

[5] Hyakudome, T. (2011). Design of Autonomous Underwater Vehicle. International Journal of Advanced Robotic Systems, 8(1), 131-139.

[6] "Remote detection and localization of gas leaks with autonomous mobile inspection robots in technical facilities" website: http://www.flir.com/cs/emea/en/view/?id=62559.

[7] Krishnaswamy Kannan and Gowtham S, "Intelligent Personal Assistant and Surveillance Robot using Zigbee Communication",International Journal of Engineering Science and Technology (IJEST), ISSN : 0975-5462 Vol. 4 No.10October 2012.